IEEE Access
Multidisciplinary | Rapid Review | Open Access Journal

Received July 8, 2021, accepted July 19, 2021, date of publication August 3, 2021, date of current version August 16, 2021.

Digital Object Identifier 10.1109/ACCESS.2021.3102380

Noise Power Properties of Magnetic Nanoparticles as Measured in Thermal Noise Magnetometry

KATRIJN EVERAERT[1,2], MAIK LIEBL[1], DIRK GUTKELCH[1], JAMES WELLS[1], BARTEL VAN WAEYENBERGE[2], FRANK WIEKHORST[1], AND JONATHAN LELIAERT[2], (Member, IEEE)

[1]Physikalisch-Technische Bundesanstalt, 10587 Berlin, Germany
[2]Department of Solid State Sciences, Ghent University, 9000 Ghent, Belgium

Corresponding author: Katrijn Everaert (katrijn.everaert@ptb.de)

This work was supported by the German Research Foundation (DFG) through the Project "MagNoise: Establishing Thermal Noise Magnetometry for Magnetic Nanoparticle Characterization" under Grant FKZ WI4230/3-1. The work of Jonathan Leliaert was supported by the Fonds Wetenschappelijk Onderzoek (FWO-Vlaanderen) with a postdoctoral fellowship.

ABSTRACT Magnetic nanoparticles have proven to be extremely useful in a broad range of biomedical applications. To ensure optimal efficiency, a precise characterization of these particles is required. Thermal Noise Magnetrometry (TNM) is a recently developed characterization technique that has already been validated against other techniques. TNM offers a unique advantage in that no external excitation of the system is required to drive the measurement. However, the extremely small stochastic signal in the femtotesla range currently limits the accessibility of the method, and a better understanding of the influences of the sample characteristics on the TNM signal is necessary. In this study, we present a theoretical framework to model the magnetic noise power properties of particle ensembles and their signal as measured via TNM. Both intrinsic sample properties (such as the number of particles or their volume) and the geometrical properties of the sample in the setup have been investigated numerically and validated with experiments. It is shown that the noise power depends linearly on the particle concentration, quadratically on the individual particle size, and linearly on the particle size for a constant total amount of magnetic material in the sample. Furthermore, an optimized sample shape is calculated for the given experimental geometry and subsequently 3d printed. This geometry produces a 3.5 fold increase in TNM signal (0.007 to 0.026 pT^2) using less than half of the magnetic material considered in the intial measurements.

INDEX TERMS Biomedical material, magnetic properties, magnetic nanoparticles, magnetic noise, thermal noise.

I. INTRODUCTION

Thermal fluctuations are ubiquitous in a broad range of physical systems. Although they are often unwanted and referred to as noise, they also carry information. Einstein was the first to model the thermal movements of colloidal particles in a fluid [1], more commonly known as Brownian motion. Understanding of this phenomenon underpins the technique "Dynamic Light Scattering" (DLS), a powerful characterization method for macromolecular systems [2], [3]. The thermal agitation of electrons in a conductor (Johnson-Nyquist noise) [4], [5] has also been implemented in applications such as Johnson noise thermometry [6], [7]. This technique is especially relevant in low-temperature systems because no electric current is required to drive the measurement, thereby minimizing heat dissipation in the sample [8], [9]. A general theory on thermal noise has been formulated in the fluctuation-dissipation theorem (FDT) [10], [11]: the fluctuations in any extensive quantity are related to the dissipation in the system as a result of the application of its conjugate intensive quantity [12]. Although these theories and applications have been established for decades, the study of thermal fluctuations and the FDT continues to be an active research field today, with several applications in various disciplines.

The associate editor coordinating the review of this manuscript and approving it for publication was Chaitanya U. Kshirsagar.

For example, the FDT has been extended to non-equilibrium and non-Hamiltonian systems [13], allowing the response of a climate system to a weak external force to be modelled [14]–[17]. Johnson noise thermometry can also provide a basis for the experimental determination of the Boltzmann constant [18]–[20] which is used for the definition of the kelvin.

In this paper magnetic nanoparticle (MNP) dynamics are discussed. Their dynamic properties are inherently stochastic due to the particles' nanoscale sizes. The MNPs typically consist of a magnetic core (normally iron oxide) and a non-magnetic shell (for example, silica). Over the last few decades they have been implemented in numerous biomedical applications [21], [22]. The MNP can be imaged directly using magnetic particle imaging [23]–[25] (MPI) or Magnetorelaxometry imaging [26]–[28] (MRXi), or can be used as a contrast agent [29] in magnetic resonance imaging (MRI). MNPs can serve as heat generators in cancer treatment (magnetic field hyperthermia) [30], [31] and can be used in targeted drug delivery [32]. For these applications to function safely, reliably and efficiently there is a need for accurate MNP characterization. Important properties to determine include the size distribution of the MNPs and their related dynamic properties.

All established direct magnetic characterization techniques rely upon a measurement of the particles' response to an externally applied field [33]. For example, Magnetorelaxometry [34] (MRX) is a MNP characterization technique in which the relaxation of the net magnetic moment of a nanoparticle sample is recorded, after abruptly switching off an externally applied magnetic field. This method is an example of the dissipation part of the FDT: the dissipation or impedance of the magnetization M of the sample, the extensive quantity, is studied when an externally applied field H is applied, the intensive quantity. However, the external field excitation could potentially alter the particles magnetization state [35], [36] and therefore influence the outcome of the measurement. The FDT shows that the thermal fluctuations in M in the absence of any external field are caused by the very same mechanisms as those responsible for the dissipation. The fluctuations can thus also be used to characterize nanoparticle systems. The technique of Thermal Noise Magnetometry (TNM) has been introduced by Leliaert *et al* in Ref. 37 and validated against MRX in Ref. 38. It is a powerful alternative for the characterization of magnetic nanoparticles, without impact on the magnetic state of the sample. Further improvement of this method will provide fundamental insight into the magnetization dynamics of MNP and facilitate their precise characterization for biomedical applications.

On the timescale of a typical MNP characterization measurement, the MNP dynamics are driven by two different stochastic processes. Together, they give rise to the relaxations observed in MRX, and likewise the fluctuations considered in TNM. MRX and TNM thus share the same characteristic timescale. First, there is the Néel switching process. In this process, the magnetic moment of the MNP changes direction by crossing the energy barrier KV_c set by the magnetocrystalline (or shape) anisotropy of the particle, with anisotropy constant K and the volume V_c of the magnetic core. The Néel fluctuation time τ_N is given by [39]

$$\tau_\mathrm{N} = \tau_0 \exp\left(\frac{KV_c}{k_\mathrm{B}T}\right). \tag{1}$$

τ_0 is the inverse of the attempt frequency, typically estimated on the order of 10^{-9} s [40], [41]. In a suspension, the particles can also rotate mechanically. This process is called Brownian rotation. In contrast to the Néel relaxation, the magnetization is fixed within the frame of the particle and rotates together with the particle in the detectors' frame of reference. The Brownian fluctuation time τ_B is given by [42]

$$\tau_\mathrm{B} = \frac{3\eta V_\mathrm{h}}{k_\mathrm{B}T}, \tag{2}$$

where V_c and V_h denote the core and hydrodynamic volume of the particle respectively, and η is the viscosity of the suspension.

The combined relaxation of a system in which both Néel and Brownian processes are occurring is described by the effective fluctuation time τ_eff. This is given by the inverse sum of the Néel and Brownian fluctuation times

$$\tau_\mathrm{eff} = \frac{\tau_\mathrm{N}\tau_\mathrm{B}}{\tau_\mathrm{N} + \tau_\mathrm{B}} \tag{3}$$

and is generally dominated by one contribution, depending on the particles' size [43].

Without the application of an external magnetic field, the magnetization dynamics of the nanoparticle system can be characterized by means of the thermal fluctuations: the thermal magnetic noise. However, the signal measured in TNM is inherently extremely small (down to a few fT), which makes the characterization of low concentration samples very time consuming or even impossible. Moreover, the stochastic nature of the experiment makes the interpretation of the results less intuitive. Therefore, development of the TNM method will benefit from a deeper understanding of the measured signal and its dependence on the sample configuration. In this work, we present a theoretical framework constructed to mirror our TNM experiment. Its usage is twofold: first it allows us to investigate the influence of different sample parameters on the TNM signal, thereby making the design of future experiments and the interpretation of future results more accessible. Second, it can be used to improve our experiment by calculating an optimized sample shape for the given geometrical constraints. The numerical results are verified with experiments.

First, two methods of calculating the thermal noise power are described and validated. Their use in the context of TNM measurements and simulations are then presented. Next, the dependence of the noise power on two sample parameters is studied: the number of particles and their size. Finally, the influence of the volume, distance and geometry of the sample with respect to the detector is presented, and a

comparison between the optimized and conventional sample shapes is made in terms of TNM signal.

II. METHODS

A. THERMAL NOISE MAGNETOMETRY

TNM measures fluctuations in the magnetic flux density originating from changes in the direction of the particles' magnetic moments due to thermal energy in the system. The magnetic flux density B^{λ} at a certain point in space and in a certain direction is a stochastic variable, where λ is one specific realization of the magnetic moments' phase space Ω. B^{λ} is a superposition of all the magnetic field contributions of the magnetic moments of the different particles in the sample. Because the magnetic moment of every particle is free to move in any direction on the unit sphere, Ω is uncountable. B^{λ} is described by the probability density function $P_B(x)$, where x is a parameter representing a realization of Ω. Any statistical average of a function f on the nanoparticle ensemble is then calculated as:

$$\langle f(B^{\lambda})\rangle = \int f(B^{\lambda})P_B(x)dx \tag{4}$$

At non-zero temperatures, the magnetization direction of each nanoparticle changes over time. Consequently, B^{λ} is also a time dependent stochastic process. In this work it is assumed that the thermal fluctuations in the magnetic signal $B^{\lambda}(t)$ of a nanoparticle ensemble is stationary and ergodic: this means that the statistical ensemble averages do not change over time and can be set equal to their time averages:

$$\langle f(B^{\lambda})\rangle = \overline{f(B^{\lambda}(t))} = \lim_{T\to\infty}\left[\frac{1}{T}\int_0^T f(B^{\lambda}(t))dt\right] \tag{5}$$

For stationary and ergodic processes, the link between theory (what can be calculated) and experiments (what can be measured) can readily be made. The ensemble averages (the average of $B^{\lambda}(t^*)$ over the configurations λ at fixed time t^*) are most suitable for the theoretical calculations, whereas the time averages, i.e. the average of one realization λ^* of the stochastic process $B^{\lambda^*}(t)$ over time, are much more practical to record in experiments [12].

There are two important quantities for the stochastic process $B^{\lambda}(t)$. First, its autocovariance is given by

$$\begin{aligned}\Gamma_{BB}(t_1,t_2) &= \langle B^{\lambda}(t_1)B^{\lambda}(t_2)\rangle - m_x(t_1)m_x(t_2)\\ &= \Gamma_{BB}(\tau) = \langle B^{\lambda}(t_1)B^{\lambda}(t_1+\tau)\rangle - m_x^2,\end{aligned} \tag{6}$$

where $m_x(t)$ is the statistical average of B^{λ} and the second equality holds for stationary processes, as t_2-t_1 is substituted by τ. Secondly, its Power Spectral Density (PSD) is defined as

$$S_b(f) = \lim_{T\to\infty}\frac{1}{T}\int_0^T \langle|B^{\lambda}(t)\exp(-i2\pi ft)dt|^2\rangle \tag{7}$$

which takes the form of a Lorentzian for a monodisperse magnetic nanoparticle ensemble [44]:

$$S_b(f) \propto \frac{(4\tau_{\text{eff}})^{-1}}{(\pi f)^2 + (2\tau_{\text{eff}})^{-2}} \tag{8}$$

This spectrum is characterized by a white noise part up to the cutoff frequency $1/(2\tau_{\text{eff}})$ and a $1/f^2$ dependence for frequencies larger than the cutoff frequency [37]. The amplitude of the power spectrum follows a $1/d^6$ power law, where d is the distance between the MNPs and the point of the magnetic field detection. For particle ensembles with an extended size distribution, the PSD is a superposition of Lorenzians [38] whose shape depends on the corresponding fluctuation time distribution.

By measuring the stochastic signal $B^{\lambda}(t)$ and analysing its spectrum, it is possible to reconstruct the particle size distribution. Because the fluctuations are inherent to the particles and only depend on their properties and the thermal energy in the system, no external excitation has to be applied to the ensemble during the measurement.

B. NOISE POWER CALCULATION

To enable quantitative comparison between different sample configurations, the total thermal noise power P measured in the detector was selected as the basis for analysis. The noise power takes both changes in the shape and the amplitude of the PSD into account, and is therefore a suited parameter to investigate both the influence of intrinsic particle parameters and the sample geometry. We elaborate on two different methods to calculate the noise power [12] in the context of TNM: by calculating the variance over different independent configurations, or by integrating the PSD over its full frequency range. The first methods will be the fastest for the simulations, while the second method is preferred for experiments. The consistency between both calculation methods is verified in the results and discussion sections.

1) METHOD 1: CONFIGURATION AVERAGE OF THE VARIANCE

The instantaneous noise power of the stochastic process $B^{\lambda}(t)$ is given by its variance

$$P_b(t) = \langle B^{\lambda}(t)B^{\lambda}(t)\rangle \tag{9}$$

which is independent of t for stationary processes. Calculating the statistical average is not possible without knowing the probability density function. The law of large numbers can therefore be used to approximate the statistical average:

$$\langle (B^{\lambda})^2\rangle = \lim_{n\to\infty}\frac{(B^{\lambda(1)})^2 + (B^{\lambda(2)})^2 + \ldots + (B^{\lambda(n)})^2}{n} \tag{10}$$

If n is large, the average of the squared magnetic flux density from n random configurations λ of Ω is a good approximation to estimate the magnetic noise power. The variance of a stochastic signal is also used in other disciplines as a parameter to characterize the system [45], [46] or to track thermal noise power changes over time [47].

2) METHOD 2: PSD INTEGRATION

It is generally cumbersome or impossible to prepare a large number of uncorrelated experiments. Often, there is only one realization λ, which is evaluated over time. Measuring the

noise power based on (10) as a statistical average is thus experimentally unfeasible. By assuming that the process is stationary and ergodic, the ensemble averages can be replaced by time averages. Conveniently, the same assumptions also enable the use of the Wiener–Khinchin theorem [48], [49], which states that the autocovariance and the power spectral density are each other's Fourier transforms.

$$\Gamma_{BB}(\tau) = \int_{-\infty}^{\infty} S_b(f)\exp(2\pi i f\tau)df \tag{11}$$

Because the noise power equals the autocovariance for $\tau = 0$: $P_x = \Gamma_{XX}(0)$, we can write

$$P_b = \Gamma_{BB}(0) = \int_{-\infty}^{\infty} S_b(f)df\,. \tag{12}$$

This means that the noise power can also be calculated by integrating the PSD over the full frequency range. The contributions of all the power sources operating at different frequencies are added to yield the total power in the system. Alternatively, the noise power in a specific frequency band can be considered by changing the integration boundaries to track e.g. changes in specific dynamical ranges [50], [51].

Note that, next to the noise power and the Power Spectral Density $\left(\text{with units } fT^2 \text{ and } \frac{fT^2}{Hz} \text{ respectively}\right)$, the noise amplitude and the Amplitude Spectral Density or the RMS Spectral Density $\left(\text{with units } fT \text{ and } \frac{fT}{\sqrt{Hz}} \text{ respectively}\right)$ are also often used. Because the latter quantities are the square roots of the former, they both contain the same information. In this paper, we will work with the noise power and power spectral density.

C. THERMAL NOISE MAGNETOMETRY EXPERIMENTS

TNM experiments were performed in the MRX setup at the Physikalisch-Technische Bundesanstalt in Berlin [52]. It consists of 6 SQUID sensors with rectangular pickup coils, which are operated inside an integrated cylindrical superconducting magnetic shield. Through a warm bore with a diameter of 27 mm, the MNP sample can be positioned close to the SQUID sensors at a typical distance of 23.5 mm. For our measurements we only used one sensor. Iron oxide particles obtained from Berlin Heart GmbH with an iron concentration of 1.214 mmol/l were used as the MNP sample. This nanoparticle system has been chosen for its high noise signal, thereby allowing TNM measurements of a relatively highly diluted sample. Interparticle interactions were found to be of negligible strength for all studied concentrations of the sample and the formation of aggregates has not been observed on the timescale of the experiments. This is in line with expectations, since the non-magnetic particle shells provide stabilisation and prevent the particles from clustering.

In each TNM measurement, we recorded 9,000 sampling frames of the time signal $B^{\lambda}(t)$ with a sample frequency $f_s = 100$ kHz. Each frame consist of $N = 50,000$ sample points. The PSD of each frame was then calculated in the following way:

1) To overcome the problem of spectral leakage, each time signal x_i' is first multiplied with the Hann window function w_i ($i = 0 \ldots N-1$): $x_i = x_i' \cdot w_i$. The fast Fourier transform (FFT) is then applied on x_i to yield FFT(x_i)=a_i. Because only positive frequencies are to be considered, the Fourier amplitudes belonging to the negative frequency part are mapped to the positive frequency part. The Fourier amplitudes a_j belonging to these positive frequencies gain a factor of two [53].
2) The Power Spectral Density is then computed as

$$S_j = \frac{2\cdot|a_j|^2\cdot\eta^2}{f_s\cdot N} \tag{13}$$

η is a factor accounting for the window usage, and is equal to $\frac{2}{\sqrt{1.5}}$ for the Hann window. For a detailed explanation of the discrete PSD computation using windows we refer to Ref. 54.

The PSDs are then averaged over the 9,000 frames. The uncertainty on the PSD values was calculated from the standard deviation of the 9,000 frames.

1) NOISE POWER AND UNCERTAINTY CALCULATION

The noise power was calculated by integrating the resulting PSD over the frequency domain using method 2. Two contributions to the uncertainty ΔP on the power were taken into account. Firstly, we account for the uncertainty coming from the calculated uncertainties on the PSD [55]. Secondly, small amplitude variations in the background noise power were taken into account by measuring an empty sample and analysing its measurement data the same way as if it would have been a MNP sample.

D. THERMAL NOISE MAGNETOMETRY SIMULATIONS

The TNM simulations were performed with Vinamax [56]: an open-source macrospin simulation tool for magnetic nanoparticles, which was recently extended to simulate Brownian rotations of the particles [58]. The particles are considered spherical and uniformly magnetized. Each individual particle is approximated by a macrospin and the dynamics of the ensemble are simulated by numerically solving the stochastic Landau-Lifshitz-Gilbert equation [59], [60]. The shape of the sample holder was defined to closely resemble those used in the experiments and the magnetic field was evaluated in a rectangular region with the same dimensions as the SQUID pickup coil.

1) MAGNETIC FLUX DENSITY IN DETECTOR

For the calculation of the magnetic field density B, the detector was discretized in N points (with index j) and the magnetic flux density $\vec{B}_{ij}$ of every simulated particle i was evaluated in point j as a dipole-dipole field (see Fig. 1):

$$\vec{B}_{ij} = \frac{\mu_0}{4\pi}\left(\frac{3\vec{r}_{ij}(\vec{m}_i\cdot\vec{r}_{ij})}{|\vec{r}_{ij}|^5} - \frac{\vec{m}_i}{|\vec{r}_{ij}|^3}\right) \tag{14}$$

Here, $\vec{r}_{ij}$ denotes the vector between particle i and detector point j and $\vec{m}_i$ is the magnetization of particle i. The detector

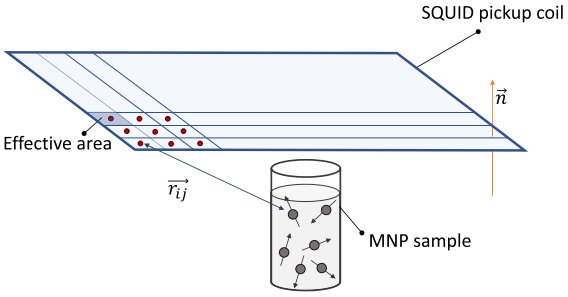

FIGURE 1. Schematic representation of the macrospin simulations modeling a TNM experiment. The particles *i* and the detector points *j* are displayed, connected through the vector $\vec{r_{ij}}$. The detector only measures the magnetic field in the direction $\vec{n}$, the normal to the detector plane. Each detector point contributes for a certain effective area, which is sufficiently small to ensure a homogeneous field in each area.

is only sensitive to fields in the direction perpendicular to its surface:

$$B_{ij} = \vec{n} \cdot \vec{B_{ij}} \tag{15}$$

where $\vec{n}$ is the normal to the detector plane. The magnetic flux density in each point j of the detector is the sum of the contributions from each particle:

$$B_j = B_{i_1 j} + B_{i_2 j} + \dots \tag{16}$$

and accounts for the magnetic flux (in Wb) through the *effective area* of this point: the area of the detector which it represents. For equidistant detector discretization, the total flux density in the full detector is then calculated by taking the average of the magnetic flux densities at the different detector points j.

III. RESULTS AND DISCUSSION

A. VALIDATION OF NOISE POWER CALCULATION METHODS

We now compare the noise power obtained using both methods presented above. To this end, we fit a volume-squared weighted lognormal particle size distribution to the spectrum measured for the iron oxide MNPs in a cylindrical sample holder, as shown in Fig. 2 (a). A lognormal distribution is commonly assumed, as this size distribution results from the magnetic nanoparticles particle synthesis process [62]. We use the following definition for the lognormal distribution, with diameter d:

$$P(d) = \frac{1}{\sqrt{2\pi}\sigma d} \exp\left(\frac{-[\ln(d/\mu)]^2}{2\sigma^2}\right) \tag{17}$$

This distribution is parameterized by μ and σ, which correspond to the median and geometric standard deviation of the distribution respectively. The mean of this distribution is given by $\exp\left(\ln(\mu) + \frac{1}{2}\sigma^2\right)$.

Note that the diameter distribution can be transformed into a switching time distribution and the weighting can be changed from a volume-squared weighted to a volume- or number weighted distribution, as described in the appendix.

The size distribution fitted from the TNM data had parameters $\mu = 46.1 \pm 0.5$ nm and $\sigma = 0.64 \pm 0.01$, corresponding to a mean diameter of 56.6 nm. The sample has also been measured with MRX and DLS as control measurements, yielding an average particle diameter of 54.7 nm and z-average of 55.0 nm respectively. Both values are in excellent agreement with the value obtained from the TNM data. This distribution was subsequently used to simulate a MNP ensemble using Vinamax. Each simulation contained 10,000 particles. Only Brownian switching was taken into account, and we used the material parameters of iron oxide (saturation magnetization M_s =400 kA/m) and the suspension parameters for water (viscosity $\eta = 1$ mPa·s). Since particles with a diameter smaller than 10 nm have a cutoff frequency well above the Nyquist frequency of the experiment, their characteristic Power Spectral Density is constant in the measured frequency region. As they cannot be distinguished in this measurement, they have been left out of the simulation. In future research, the experimental sample frequency of 100 kHz could be increased to make TNM also sensitive to smaller particles or, as suggested by Ref. 38, the viscosity of the suspension could be increased to lower the cutoff frequency of the particle system.

A large number of randomly chosen configurations λ are easily generated in simulations, which allows one to calculate the noise power using method 1. Generating 80,000 sample configurations, the noise power was calculated with equation (10) to be $(1.21 \pm 0.03) \cdot 10^{-6}$ fT^2. The distribution of the magnetic flux density B^λ in the detector is shown Fig. 2 (b). As expected for the lognormal size distribution, the magnetic noise is slightly non-Gaussian.

It is also possible to generate a time series of the MNP dynamics in Vinamax, similar as the time signal recorded in experiments. A video, displaying the time dependent magnetic field in the detector plane is available as supplementary material. The simulated time signal makes it possible to estimate the noise power according to method 2. This result can be quantitatively compared to the noise power found by method 1. The averaged Power Spectral Density from such a simulated signal is shown in Fig. 2 (c). Note that its amplitude does not match the amplitude of the experimental PSD in panel (a), since only 10,000 particles were considered in the simulation. The analytical expression of the PSD for the corresponding size distribution is also plotted, and an extrapolation towards the lower frequency part is made. The integration of the combined PSD (i.e. the simulated and extrapolated part up to 0.01 Hz) yields a noise power of $(1.19 \pm 0.03) \cdot 10^{-6}$ fT^2.

The noise power calculated from the two methods coincide within their uncertainty intervals. Both methods therefore yield equal noise powers, and can thus be used interchangeably for TNM. It is clear that method 1 is more convenient for simulations, where independent sample configurations are easily generated, but where the generation of the time signal requires long calculation times to cover the low frequency range of the PSD. For the experiments however, the noise power calculations naturally follow method 2.

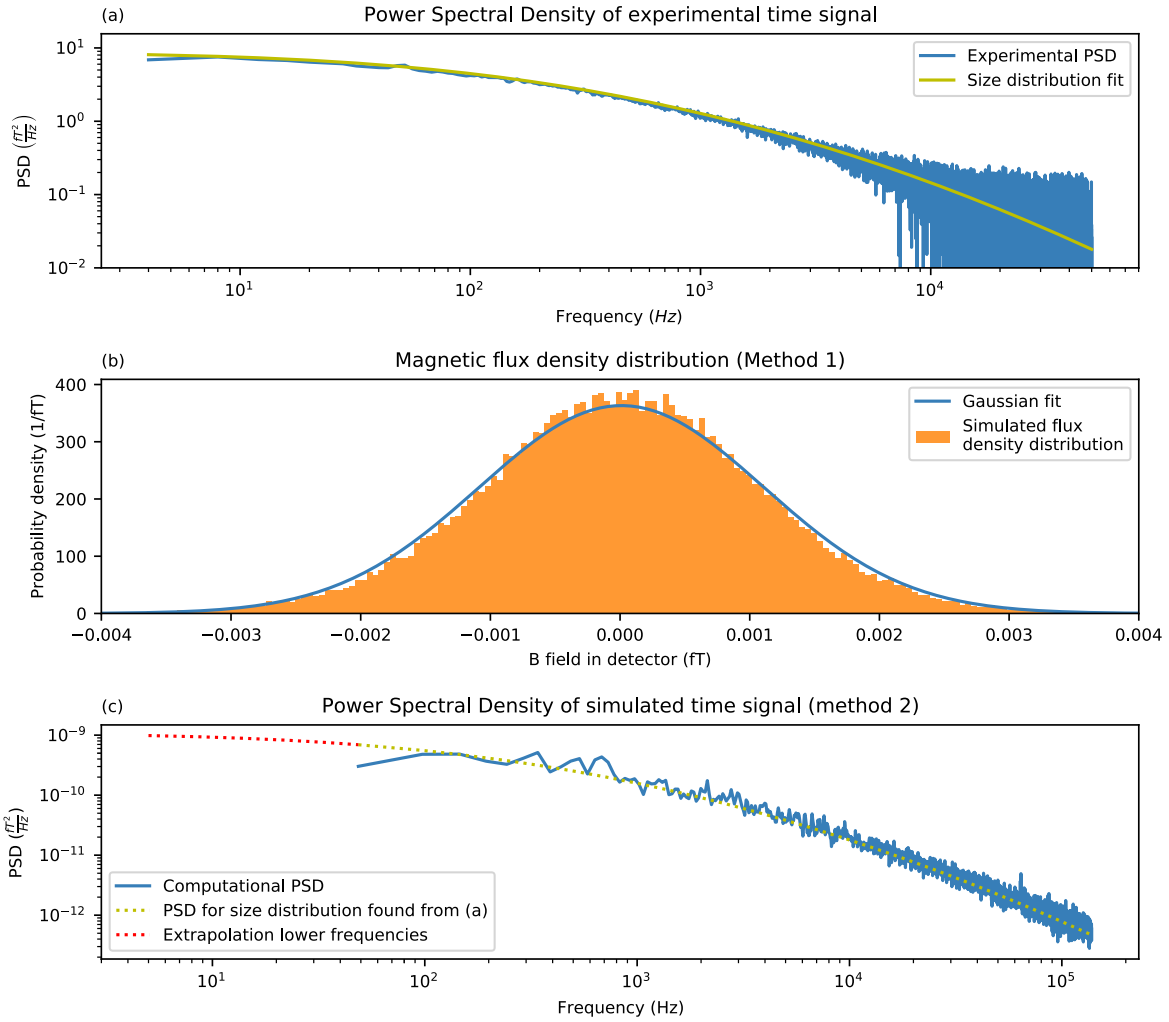

FIGURE 2. Power Spectral Density of the experimental time signal and fitted lognormal distribution (a). This size distribution is subsequently used in the simulations to validate the two noise power calculation methods. Panel (b) displays the thermal magnetic field distribution in the detector of 100,000 simulated configurations (method 1). The distribution of the stochastic magnetic signal deviates slightly from a Gaussian distribution. The Power Spectral Density of the computational time signal generated with Vinamax is displayed in (c), which is used to calculate the noise power following method 2. An extrapolation of the calculated PSD in the lower frequency range is plotted, using the PSD form of the assembling size distribution.

B. NOISE POWER DEPENDENCE ON PARTICLE VOLUME AND NUMBER OF PARTICLES

Now that it has been shown that the TNM noise power can be calculated efficiently both for simulations and experiments, the simulations can be used to improve the experiment. The number and volume of particles are two main parameters whose influence on the signal strength are well understood in other characterization methods. The stochastic nature of the TNM experiment makes their impact however less intuitive. Here, we investigate the dependence of the thermal noise power on the number of particles and their volume, both for a variable and a fixed total iron concentration. For these simulation, a cylindrical sample holder geometry has been used.

1) VARIABLE IRON CONCENTRATION

Fig. 3 shows the dependence of the noise power on the number of monodisperse particles obtained by simulations (with a fixed volume, equivalent to a radius of 60 nm) in panel (a) and the effect of the particle volume (for a fixed number of 10,000 particles) in panel (b). Note that in both cases, the total iron amount is not constant.

The noise power scales linearly with the number of particles, and quadratically with their volume. These power laws can be explained as follows. The magnetic nanoparticles in the sample are noise sources, which means that adding an additional particle to the ensemble can either result in a positive or a negative contribution to the magnetic field in the detector, depending on the orientation of the particle's magnetic moment. On average, when doubling the number of particles the flux density in the detector will only increase by a factor $\sqrt{2}$, and the noise power will scale linearly with the number of particles. This contrasts with deterministic processes like e.g. MRX measurements where all particles are aligned by an externally applied field [34]. Here, the signal amplitude scales linearly and hence the power scales

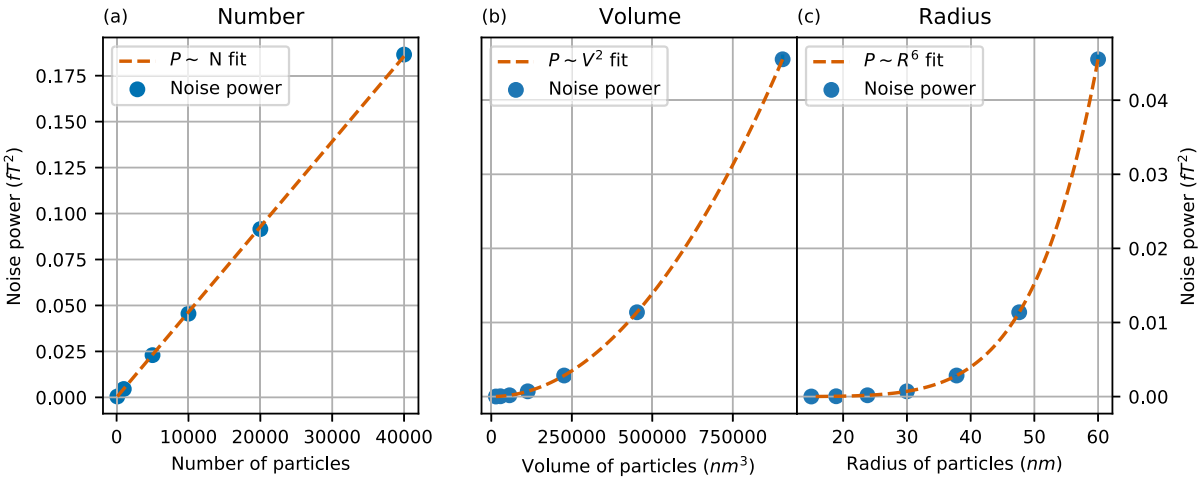

FIGURE 3. Noise power for a variable total iron amount as a function of (a) the number of particles (with a fixed volume) and (b) the volume of the particles (with a fixed number of particles). A cylindrical sample holder with monodisperse MNPs has been used. The noise power scales linearly with the number of particles and quadratically with their volume. The latter is also shown as function of particle radius in (c), based on the same dataset. Note that uncertainties have been calculated, but are too small to be seen.

quadratically with the amount of particles. These finding are in accordance with those in other stochastic systems, e.g. the scaling of the average translation distance with the square root of the number of steps in a random walk [61] (where the average translation distance and the number of steps resemble the noise amplitude and the number of particles respectively) and the linear dependence of the noise power of synchrotron radiation on the number of particles in the bunch [57].

Increasing the particles' volume while the number of particles remains constant, increases the TNM signal like in a deterministic signal. No extra noise sources are created, and an increase in the magnetic moments results in a quadratic increase of the noise power, as shown in Fig. 3 (b) and (c).

The linear dependence of the noise power on the number of particles was experimentally confirmed and shown in Fig. 4. We measured a dilutions series of the iron oxide MNPs in a water suspension. The Power Spectral Density of each dilution and their integrated noise power are shown in panels (a) and (b) respectively. The peaks observed at 50 Hz and a few higher frequencies are artefacts and have not been taken into account when calculating the total noise power. To allow a quantitative comparison, the simulation of Fig. 3 (a) was repeated for a lognormal size distribution with the parameters found from the fit in Fig. 2 (a). The results are shown in Fig. 4 (c). The total amount of particles in the sample can then be estimated from a quantitative comparison between the computational results of Fig. (b) and (c). Taking into account the linear dependence on the amount of particles, the non-diluted sample (1:1) is estimated to contain about $6 \cdot 10^{13}$ particles.

2) FIXED IRON CONTENT

Fig. 5 shows the noise power of a simulated particle ensemble in which the number of particles N and their volume V_p are varied according to $V_{tot} = N \cdot V_p$ for a fixed V_{tot}. All panels display the same data set and show that the noise power depends linearly on the particle volume and inversely on the number of particles. This is readily understood from the power laws described in the previous paragraph: for a variable particle amount, when increasing the amount of particles by a factor X, the noise power also increases by the same factor. However, because the total iron concentration is fixed, the particle volume is reduced by X. This leads to a reduction of a factor X^2 of the noise power. Together, this results in an inverse linear, and a linear relation between the noise power and the particle number and volume, respectively. This means that in a dynamic measurement where the signal is tracked over time, clustering of the particles could be observed as an increase in noise power due to a decrease in the number of particles in favour of larger particle volumes.

C. NOISE POWER DEPENDENCE ON GEOMETRICAL SETUP PARAMETERS

This section focuses on the effect of adjusting the volume, geometry and distance of the sample with respect to the detector. The magnetic field of a (point) dipole decays as $1/r^3$ with distance r. Therefore, the distance of the MNPs from the detector has a major influence on the amplitude of the TNM signal. The sample should ideally be positioned as close to the detector as possible. Additionally, the shape of the sample holder also influences the amplitude of the signal. Symmetrically shaped sample holders (cylinders, cones) are typically used. These are easy to manufacture, but may not have the optimal shape with respect to the signal strength. Therefore, we calculated a geometry and designed a sample holder that enhances the TNM signal in the given setup, taken into account both the distance from the detector and the shape of the sample holder. The signal of a conventional cylindrical sample holder is compared to that of the newly calculated geometry by constructing a sensitivity profile through the

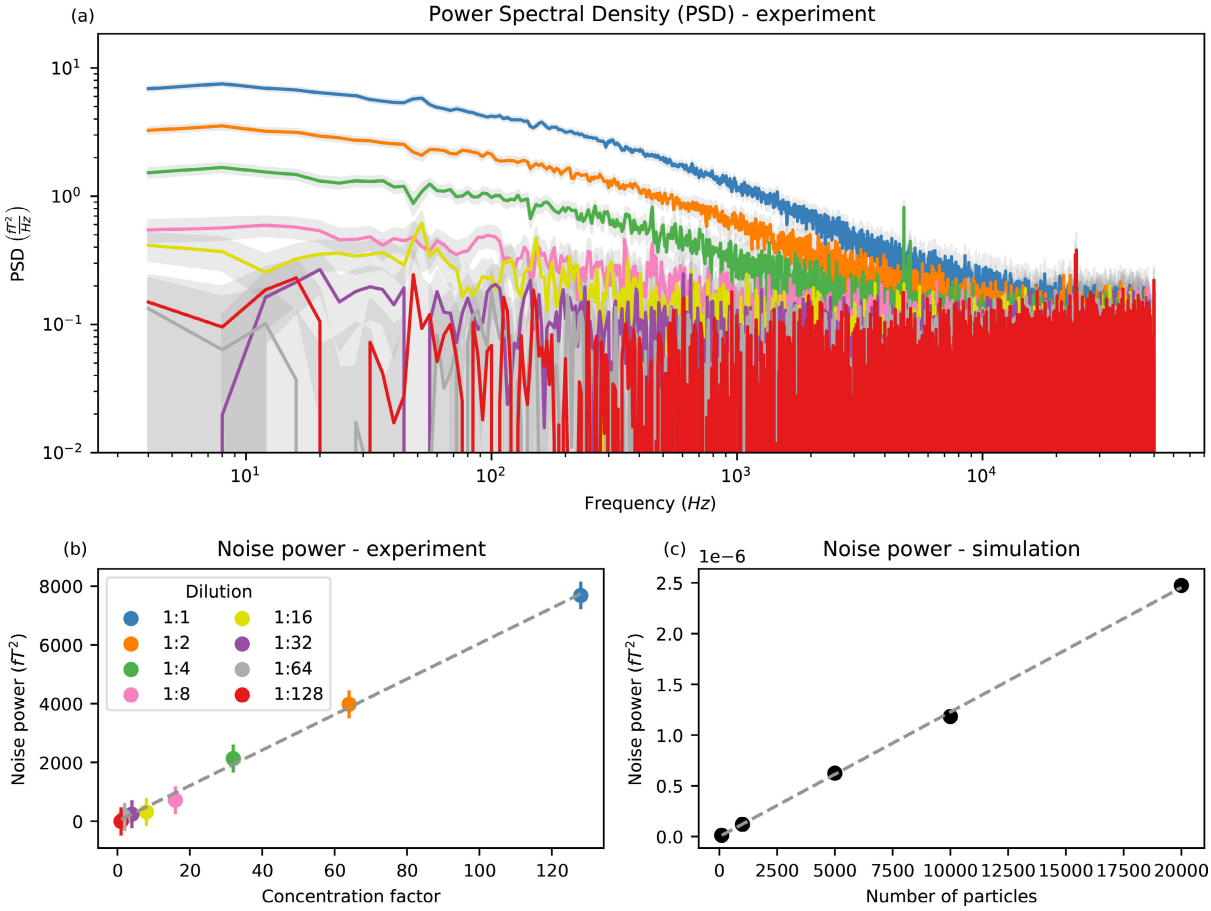

FIGURE 4. Experimental confirmation of the linear dependence of the noise power on the number of particles. (a) The measured Power Spectral Density of the dilution series and (b) their integrated noise power as a function of the concentration factor, i.e. the inverse dilution factor. Panel (a) and (b) share the same legend. (c) shows the simulated noise power as a function of number of sample particles, where the particles' size distribution is chosen to resemble the experiment.

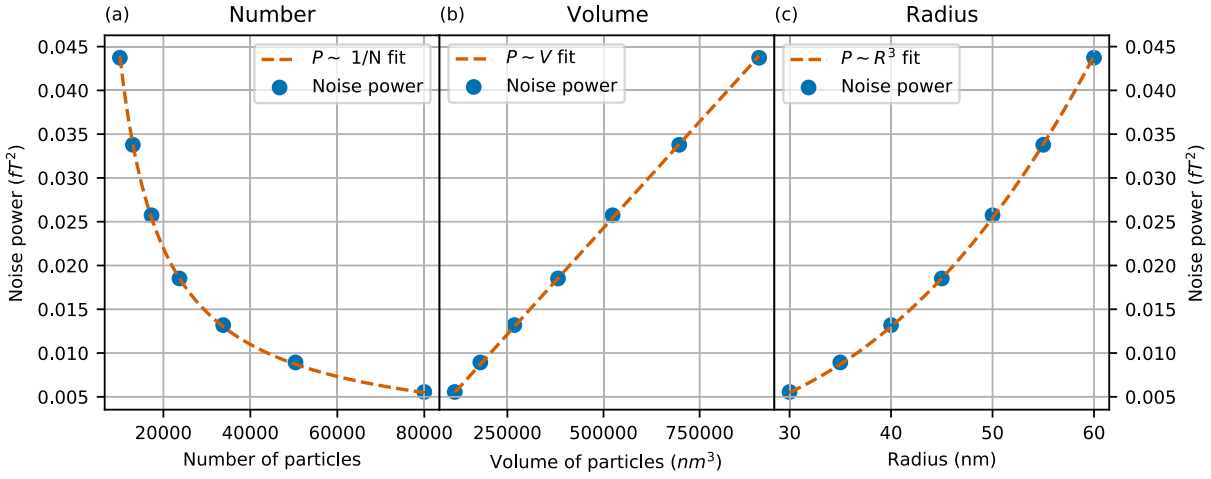

FIGURE 5. Noise power for a fixed total iron amount (fixed total volume) as a function of (a) the radius of the particles, (b) the number of particles and (c) the volume of the particles. A cylindrical sample holder with monodisperse MNPs has been used.

accessible sample space, i.e. at different distances from the detector.

The optimized geometry was calculated by discretizing the available sample space in the warm bore into a regularly spaced grid of voxels, spaced 500 μm apart. For each voxel, the hypothetical contribution of one MNP located inside the voxel to the total noise power measured in the detector was calculated. The resulting ranking of the voxels by their impact

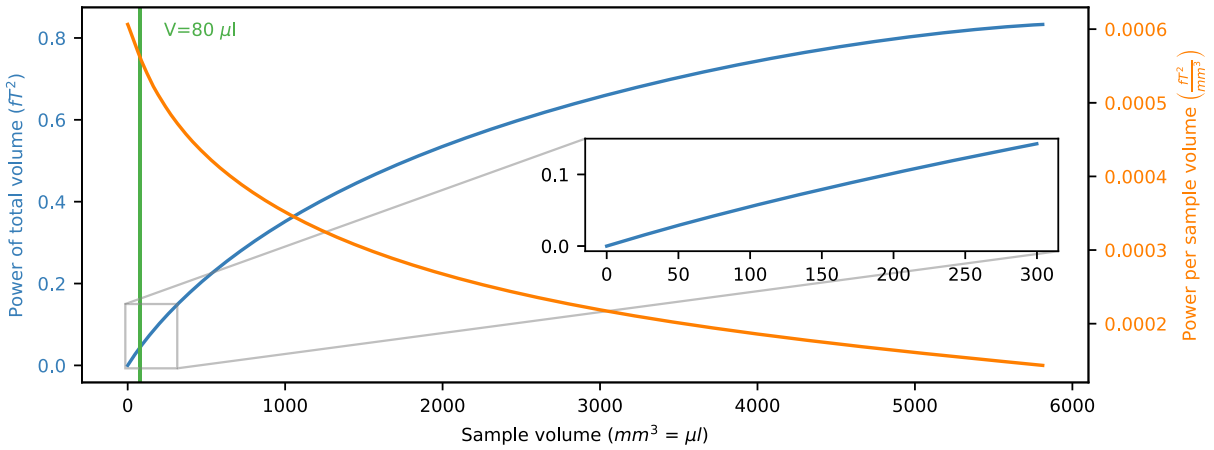

FIGURE 6. Calculated noise signal (blue) and noise power gain per added volume element (orange) as a function of the sample volume. A quasi linear regime for the noise power is visible for common sample volumes (up to 300 μl). The geometry of the 80 μl sample was used for the construction of a sample holder optimized for the experiments.

on the measured signal allowed the selection of those voxels with the highest impact when defining an optimized sample geometry for a specific volume.

Fig. 6 shows the total noise power as a function of the sample volume for the optimized sample geometry (blue curve), and displays a monotonically increasing behavior. However, the rate of increase slows down at larger volumes because points that are located at larger distances from the detector contribute little to the TNM signal. This is also reflected in the power per sample volume, as plotted in orange in Fig. 6. The most ''efficient'' sample, corresponding to the highest noise power per sample volume, would theoretically consist of only a single MNP. Although the fluctuations of individual particles can be captured [63], the noise power would be insufficient to be detected in our setup, as it was designed to characterize magnetic nanoparticle samples containing over 10^9 particles. Because the smooth decrease of the orange noise power per volume, there is no clear cutoff value for the sample volume. Instead, bearing in mind the cost of the material and practicality of the measurements, we chose to optimize our experimental sample holder geometry for a volume of 80 μl. This is an improvement upon the regular cylindrical sample holder which contains 200 μl sample material.

One way to further increase the signal per sample volume would be to use all 6 detectors of the setup. Instead of placing the entire sample as close as possible to one detector, the volume could be divided into 6 sub-volumes divided over the 6 detectors. However, because of the nearly linear $P(V)$ curve for small volume changes V (see the inset of Fig. 6), such a construction would barely increase the noise power for these volumes and would significantly increase the sample preparation time. Therefore, only one detector was used for the construction of our optimized sample holder.

1) SENSITIVITY PROFILES

The two sample holders are now compared by their noise power profile, as recorded at different position along the warm bore axis. This is referred to as the sensitivity profile in the remainder of this paper. The experimental and numerical sensitivity profiles are presented in Fig. 7, in which the conventional and the optimized sample holder are called ''SH 1'' and ''SH 2'', respectively. The simulations have been made for 10,000 sample configurations with the lognormal size distribution parameters as shown in Fig. 2 (a). To enable direct comparison, the numerical sensitivity curve has been re-scaled with the average ratio of the experimental and simulated profile.

Fig. 7 shows a qualitative agreement between the numerical and experimental sensitivity profiles. The experimental curves typically display slightly sharper peaks, i.e. higher values around position 0 and lower values in the tails at larger distances. The ratios between the experimental and the computational noise power at distance zero are 1.07 and 1.06 for the optimized and the cylindrical sample holders, respectively. This small difference is attributed to a systematic inaccuracy, e.g. a small difference between the theoretical and the actual length of the detector in the experiment. Nonetheless, the good qualitative agreement between the experimental and simulated results validates the computational framework used to simulate the thermal noise of the magnetic particles.

Another conclusion that can be drawn from Fig. 7 is that the geometrical parameters of the sample can be numerically optimized in favor of the TNM signal. At the optimal depth, a factor of 3.5 in signal strength is gained for the optimized sample holder compared to the regular cylindrical one, this is achieved despite the volume of the magnetic material having been reduced by more than half. The aforementioned procedure enables to precisely define an ideal TNM sample holder shape for to the detector geometry of any experimental setup.

As a guide to the eye, the experimental curves are fitted with a dipole-dipole sensitivity profile model:

$$P_b = a\left(\frac{1}{(d^2+b^2)^3} + \frac{1}{(d^2+b^2)^5}\right) \tag{18}$$

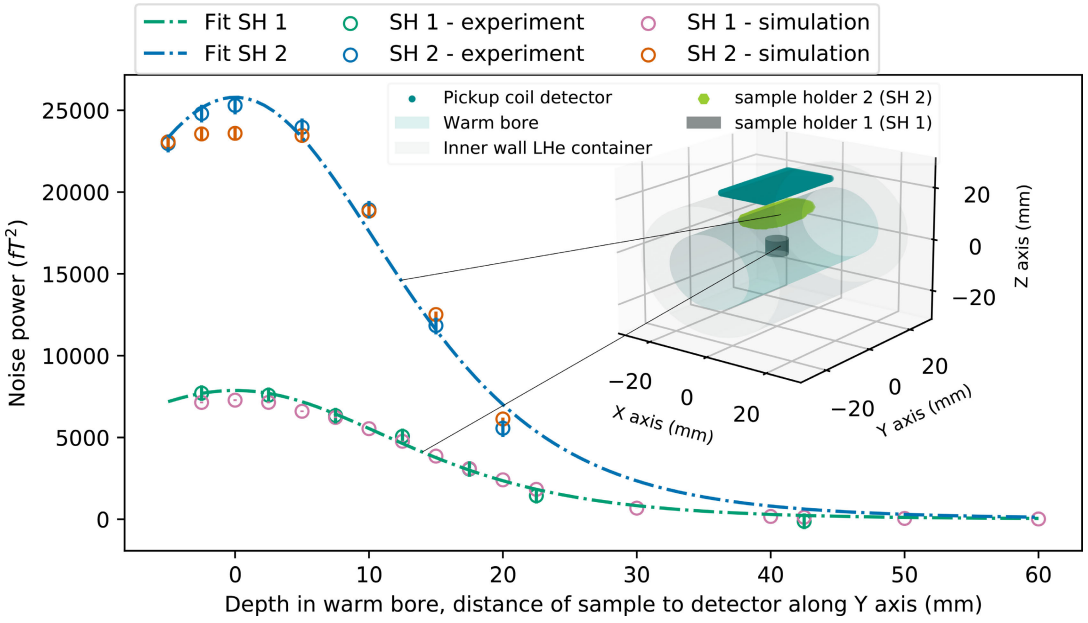

FIGURE 7. Sensitivity profile of the conventional (SH 1) and the optimized (SH 2) sample holders, both measured experimentally and computationally. By varying the y-coordinate of the sample holders, thereby altering the distance to the detector, a noise power sensitivity profile is constructed as a function of the position of the sample holder in the warm bore. The values of the simulations are scaled in order to match the experimental values. The experimental curves are fitted with the dipole-dipole sensitivity profile (18). The shapes of the two sample holders in the experimental setup are shown in the inset.

where P_b is the noise power, d the position in the warm bore, b the distance between the sample and the detector and a a weight factor (which could for example account for the amount of particles in the sample). For the cylindrical sample holder, the dipole fit matches the data quite well, due to the relatively large distance between the sensor and the narrow cylinder. From the geometry shown in the inset of Fig. 7 it is obvious that a simple point-point model between the detector and the optimized sample holder is not a good approximation.

IV. SUMMARY AND CONCLUSION

A theoretical and numerical framework to examine the noise power properties of magnetic nanoparticle ensembles has been reported as measured in TNM. This magnetic nanoparticle characterization technique provides a method to derive the size distribution of the ensemble by measuring the thermally induced fluctuations in the magnetic field. In contrast to other magnetic characterization methods, no external magnetic fields need to be applied. This can be beneficial as an applied field can potentially change the magnetic state of the particles. However, the signal measured in TNM is inherently small (down to fT range) and stochastic in nature, limiting the current accessibility of the method and making the results non-intuitive for interpretation. The dependence of the TNM signal on basic, yet fundamental, sample parameters has been studied numerically and verified with experiments. It has been shown that the noise power depends linearly on the particle concentration, quadratically on the individual particle size, and linearly on the particle size for a constant total amount of magnetic material in the sample. An optimized sample shape has been calculated and constructed, which has been compared with a conventional sample holder by measuring a sensitivity profile in the experimental setup. The optimized shape showed an increase in TNM signal by a factor of 3.5 (from approximately 0.007 to 0.026 pT^2), while the amount of magnetic material is reduced with more than half of the volume of the conventional holder. The qualitative correspondence between the numerical and experimental profiles validates the numerical framework and proves the self-consistency of the approach. The simulations make it possible to predict and visualize aspects of TNM which can subsequently be analyzed and studied experimentally. Our results therefore contribute to the establishment of TNM as a reliable magnetic nanoparticle characterization method, thereby paving the way towards improved fundamental insights in the magnetization dynamics of magnetic nanoparticle ensembles.

A. APPENDIX

The TNM Power Spectral Density consists of a (volume-squared) weighted sum of Lorentzian curves (see 8), each corresponding to the noise spectrum of a single nanoparticle. This signal can be decomposed in a, commonly used [62], lognormal distribution of such curves, as described by

$$P(x, \mu, \sigma^2) = \frac{1}{\sqrt{2\pi}\sigma x} \exp\left(\frac{-[\ln(x/\mu)]^2}{2\sigma^2}\right). \quad (19)$$

However, often the *relaxation time* distribution is less useful than the corresponding *diameter* distribution, which itself can be either number, volume or volume-squared weighted.

This appendix will derive and recall some useful properties of the lognormal size distribution in order to perform these transformations.

Note that there is a fundamental difference between transforming the volume and number weighted diameter distributions into each other, and the transformation of the (e.g. volume weighted) diameter distribution into the (e.g. also volume weighted) switching time distribution.

The first transformation seeks to describe two *different* distributions as function of *the same* quantity, i.e. diameter. In contrast, the second transformations describes *the same* distribution as function of *different* quantities, i.e. diameter or switching time.

B. TRANSFORMING A NUMBER WEIGHTED DISTRIBUTION INTO A DIAMETER WEIGHTED DISTRIBUTION AND VICE VERSA

In Ref. 64, it is shown for the lognormal size distribution how to transform a volume weighted distribution into a number weighted distribution. Here, this result is extended to a volume-squared weighted distribution:

$$D^6 \overbrace{P(D,\mu,\sigma^2)}^{\text{number weighted}} dD \propto D^3 \overbrace{P(D,\exp[\ln(\mu)+3\sigma^2],\sigma^2)}^{\text{volume weighted}} dD \propto \overbrace{P(D,\exp[\ln(\mu)+6\sigma^2],\sigma^2)}^{\text{volume}-\text{squared weighted}} dD \tag{20}$$

C. TRANSFORMING A SWITCHING TIME DISTRIBUTION INTO A DIAMETER DISTRIBUTION AND VICE VERSA

$$P(\tau_B,\mu_\tau,\sigma_\tau^2)d\tau_B \propto P\left(D,\left[\frac{2k_BT}{\eta\pi}\mu_\tau\right]^{1/3},\frac{\sigma_\tau^2}{9}\right)dD \tag{21}$$

and

$$P(D,\mu_D,\sigma_D^2)dD \propto P\left(\tau_B,\frac{\pi\eta}{2k_BT}\mu_D^3,9\sigma_D^2\right)d\tau_B \tag{22}$$

where the following properties of the lognormal distribution were used [64]:

Multiplication with a scalar a: if variable x is lognormal distributed with mean μ and standard deviation σ, then $y = a \cdot x$ is lognormal distributed with mean $a\mu$ and standard derivation σ.

$$P(x,\mu,\sigma^2)dx = P(y,a\mu,\sigma^2)dy \tag{23}$$

Exponentiation with a scalar a: if variable x is lognormal distributed with mean μ and standard deviation σ, then $y = x^a$ is lognormal distributed with mean μ^a and standard derivation $a\sigma$.

$$P\left(x,\mu,\sigma^2\right)dx = P\left(y,\mu^a,a^2\sigma^2\right)dy \tag{24}$$

AUTHOR CONTRIBUTIONS STATEMENT

Jonathan Leliaert and Frank Wiekhorst defined the project. Katrijn Everaert, Jonathan Leliaert, Frank Wiekhorst and Maik Liebl conceptualized the study. Katrijn Everaert conducted the measurements and analysed the results. Katrijn Everaert and Jonathan Leliaert performed the simulations. Dirk Gutkelch and Katrijn Everaert designed and manufactured the optimized experimental sample holder. Katrijn Everaert, Frank Wiekhorst, Maik Liebl, James Wells, and Jonathan Leliaert discussed the results and prepared the manuscript. Jonathan Leliaert, Frank Wiekhorst, and Bartel Van Waeyenberge supervised the project. All authors reviewed the manuscript.

REFERENCES

[1] A. Einstein, "Über die von der molekularkinetischen theorie der Wärme geforderte bewegung von in ruhenden flüssigkeiten suspendierten teilchen," *Annalen der Physik*, vol. 322, no. 8, pp. 549–560, 1905.
[2] B. J. Berne and R. Pecora, *Dynamic Light Scattering: With Applications to Chemistry, Biology, And Physics*. New York, NY, USA: Dover, 1976.
[3] J. Stetefeld, S. A. McKenna, and T. R. Patel, "Dynamic light scattering: A practical guide and applications in biomedical sciences," *Biophys. Rev.*, vol. 8, no. 4, pp. 409–427, 2016.
[4] J. B. Johnson, "Thermal agitation of electricity in conductors," *Phys. Rev.*, vol. 32, no. 1, pp. 97–109, Jul. 1928.
[5] H. Nyquist, "Thermal agitation of electric charge in conductors," *Phys. Rev.*, vol. 32, no. 1, pp. 110–113, Jul. 1928.
[6] D. R. White, R. Galleano, A. Actis, H. Brixy, M. De Groot, J. Dubbeldam, A. L. Reesink, F. Edler, H. Sakurai, R. L. Shepard, and J. C. Gallop, "The status of Johnson noise thermometry," *Metrologia*, vol. 33, pp. 325–335, 1996.
[7] J. F. Qu, S. P. Benz, H. Rogalla, W. L. Tew, D. R. White, and K. L. Zhou, "Johnson noise thermometry," *Meas. Sci. Technol.*, vol. 30, no. 11, 2019, Art. no. 112001.
[8] J. Beyer, D. Drung, A. Kirste, J. Engert, A. Netsch, A. Fleischmann, and C. Enss, "A magnetic-field-fluctuation thermometer for the mK range based on SQUID-magnetometry," *IEEE Trans. Appl. Supercond.*, vol. 17, no. 2, pp. 760–763, Jun. 2007.
[9] D. Rothfuss, A. Reiser, A. Fleischmann, and C. Enss, "Noise thermometry at ultra-low temperatures," *Phil. Trans. Roy. Soc. A: Math., Phys. Eng. Sci.*, vol. 374, no. 2064, Mar. 2016, Art. no. 20150051.
[10] H. B. Callen and T. A. Welton, "Irreversibility and generalized noise," *Phys. Rev.*, vol. 83, no. 1, pp. 34–40, Jul. 1951.
[11] R. Kubo, "The fluctuation-dissipation theorem," *Reports Progr. Phys.*, vol. 29, no. 1, p. 255, 1966.
[12] P. Réfrégier, *Noise Theory and Application to Physics: From Fluctuations to Information*. New York, NY, USA: Springer, 2004.
[13] U. Marini, B. Marconi, A. Puglisi, L. Rondoni, and A. Vulpiani, "Fluctuation–dissipation: Response theory in statistical physics," *Phys. Rep.*, vol. 461, pp. 111–195, Jun. 2008.
[14] C. E. Leith, "Climate response and fluctuation dissipation," *J. Atmos. Sci.*, vol. 32, no. 10, pp. 2022–2026, Oct. 1975.
[15] A. Gritsun and G. Branstator, "Climate response using a three-dimensional operator based on the fluctuation–dissipation theorem," *J. Atmos. Sci.*, vol. 64, no. 7, pp. 2558–2575, 2007.
[16] F. C. Cooper and P. H. Haynes, "Climate sensitivity via a nonparametric fluctuation–dissipation theorem," *J. Atmos. Sci.*, vol. 68, no. 5, pp. 937–953, 2011.
[17] V. Lembo, V. Lucarini, and F. Ragone, "Beyond forcing scenarios: Predicting climate change through response operators in a coupled general circulation model," *Sci. Rep.*, vol. 10, no. 1, p. 8668, Dec. 2020.
[18] J. Qu, S. P. Benz, K. Coakley, H. Rogalla, W. L. Tew, R. White, K. Zhou, and Z. Zhou, "An improved electronic determination of the Boltzmann constant by Johnson noise thermometry," *Metrologia*, vol. 54, no. 4, pp. 549–558, 2017.
[19] C. Urano, K. Yamazawa, and N.-H. Kaneko, "Measurement of the Boltzmann constant by Johnson noise thermometry using a superconducting integrated circuit," *Metrologia*, vol. 54, no. 6, pp. 847–855, Dec. 2017.

[20] D. Drung and C. Krause, "Dual-mode auto-calibrating resistance thermometer: A novel approach with Johnson noise thermometry," *Rev. Sci. Instrum.*, vol. 92, no. 3, 2021, Art. no. 034901.
[21] Q. A. Pankhurst, J. Connolly, S. K. Jones, and J. Dobson, "Applications of magnetic nanoparticles in biomedicine," *J. Phys. D, Appl. Phys.*, vol. 36, no. 13, pp. 167–181, 2003.
[22] S. Tong, H. Zhu, and G. Bao, "Magnetic iron oxide nanoparticles for disease detection and therapy," *Mater. Today*, vol. 31, pp. 86–99, Dec. 2019.
[23] B. Gleich and J. Weizenecker, "Tomographic imaging using the nonlinear response of magnetic particles," *Nature*, vol. 435, no. 7046, pp. 1214–1217, Jun. 2005.
[24] T. Knopp and T. M. Buzug, *Magnetic Particle Imaging: An Introduction to Imaging Principles and Scanner Instrumentation*. Berlin, Germany: Springer, 2012.
[25] P. Chandrasekharan, Z. W. Tay, D. Hensley, X. Y. Zhou, B. K. Fung, C. Colson, Y. Lu, B. D. Fellows, Q. Huynh, C. Saayujya, E. Yu, R. Orendorff, B. Zheng, P. Goodwill, C. Rinaldi, and S. Conolly, "Using magnetic particle imaging systems to localize and guide magnetic hyperthermia treatment: Tracers, hardware, and future medical applications," *Theranostics*, vol. 10, no. 7, pp. 2965–2981, 2020.
[26] M. Liebl, F. Wiekhorst, D. Eberbeck, P. Radon, D. Gutkelch, D. Baumgarten, U. Steinhoff, and L. Trahms, "Magnetorelaxometry procedures for quantitative imaging and characterization of magnetic nanoparticles in biomedical applications," *Biomed. Eng./Biomedizinische Technik*, vol. 60, no. 5, pp. 427–443, Jan. 2015.
[27] A. Coene, J. Leliaert, M. Liebl, N. Löwa, U. Steinhoff, G. Crevecoeur, L. Dupré, and F. Wiekhorst, "Multi-color magnetic nanoparticle imaging using magnetorelaxometry," *Phys. Med. Biol.*, vol. 62, no. 8, p. 3139, 2017.
[28] A. Jaufenthaler, P. Schier, T. Middelmann, M. Liebl, F. Wiekhorst, and D. Baumgarten, "Quantitative 2D magnetorelaxometry imaging of magnetic nanoparticles using optically pumped magnetometers," *Sensors*, vol. 20, no. 3, p. 753, Jan. 2020.
[29] S. Laurent, C. Henoumont, D. Stanicki, S. Boutry, E. Lipani, S. Belaid, R. N. Muller, and L. V. Elst, *MRI Contrast Agents*. Singapore: Springer, 2017.
[30] H. Etemadi and P. G. Plieger, "Magnetic fluid hyperthermia based on magnetic nanoparticles: Physical characteristics, historical perspective, clinical trials, technological challenges, and recent advances," *Adv. Therapeutics*, vol. 3, no. 11, Nov. 2020, Art. no. 2000061.
[31] A. Espinosa, R. Di Corato, J. Kolosnjaj-Tabi, P. Flaud, T. Pellegrino, and C. Wilhelm, "Duality of iron oxide nanoparticles in cancer therapy: Amplification of heating efficiency by magnetic hyperthermia and photothermal bimodal treatment," *ACS Nano*, vol. 10, no. 2, pp. 2436–2446, Jan. 2016.
[32] K. T. Al-Jamal, J. Bai, J. T.-W. Wang, A. Protti, P. Southern, L. Bogart, H. Heidari, X. Li, A. Cakebread, D. Asker, W. T. Al-Jamal, A. Shah, S. Bals, J. Sosabowski, and Q. A. Pankhurst, "Magnetic drug targeting: Preclinical *in vivo* studies, mathematical modeling, and extrapolation to humans," *Nano Lett.*, vol. 16, no. 9, pp. 5652–5660, Sep. 2016.
[33] F. Ludwig, D. Eberbeck, N. Löwa, U. Steinhoff, T. Wawrzik, M. Schilling, and L. Trahms, "Characterization of magnetic nanoparticle systems with respect to their magnetic particle imaging performance," *Biomedizinische Technik/Biomed. Eng.*, vol. 58, no. 6, pp. 535–545, Dec. 2013.
[34] F. Wiekhorst, U. Steinhoff, D. Eberbeck, and L. Trahms, "Magnetorelaxometry assisting biomedical applications of magnetic nanoparticles," *Pharmaceutical Res.*, vol. 29, no. 5, pp. 1189–1202, May 2012.
[35] B. Bharti, A. Fameau, and O. D. Velev, "Magnetophoretic assembly of flexible nanoparticles/lipid microfilaments," *Faraday Discuss.*, vol. 181, pp. 437–448, Jul. 2015.
[36] E. Myrovali, N. Maniotis, A. Makridis, A. Terzopoulou, V. Ntomprougkidis, K. Simeonidis, D. Sakellari, O. Kalogirou, T. Samaras, R. Salikhov, M. Spasova, M. Farle, U. Wiedwald, and M. Angelakeris, "Arrangement at the nanoscale: Effect on magnetic particle hyperthermia," *Sci. Rep.*, vol. 6, no. 1, p. 37934, Dec. 2016.
[37] J. Leliaert, A. Coene, M. Liebl, D. Eberbeck, U. Steinhoff, F. Wiekhorst, B. Fischer, L. Dupré, and B. Van Waeyenberge, "Thermal magnetic noise spectra of nanoparticle ensembles," *Appl. Phys. Lett.*, vol. 107, no. 22, Nov. 2015, Art. no. 222401.
[38] J. Leliaert, D. Eberbeck, M. Liebl, A. Coene, U. Steinhoff, F. Wiekhorst, B. Van Waeyenberge, and L. Dupré, "The complementarity and similarity of magnetorelaxometry and thermal magnetic noise spectroscopy for magnetic nanoparticle characterization," *J. Phys. D, Appl. Phys.*, vol. 50, no. 8, Mar. 2017, Art. no. 085004.
[39] L. Néel, "Théorie du traînage magnétique des substances massives dans le domaine de Rayleigh," *J. Phys. Radium*, vol. 11, no. 2, pp. 49–61, 1950.
[40] L. Bessais, L. Ben Jaffel, and J. L. Dormann, "Relaxation time of fine magnetic particles in uniaxial symmetry," *Phys. Rev. B, Condens. Matter*, vol. 45, p. 7805, Apr. 1992.
[41] J. Leliaert, A. Coene, G. Crevecoeur, A. Vansteenkiste, D. Eberbeck, F. Wiekhorst, B. Van Waeyenberge, and L. Dupré, "Regarding the Néel relaxation time constant in magnetorelaxometry," *J. Appl. Phys.*, vol. 116, no. 16, 2014, Art. no. 163914.
[42] W. F. Brown, Jr., "Thermal fluctuations of a single-domain particle," *Phys. Rev.*, vol. 130, no. 5, pp. 1677–1686, Jun. 1963.
[43] R. E. Rosensweig, "Heating magnetic fluid with alternating magnetic field," *J. Magn. Magn. Mater.*, vol. 252, pp. 370–374, Nov. 2002.
[44] S. Machlup, "Noise in semiconductors: Spectrum of a two-parameter random signal," *J. Appl. Phys.*, vol. 25, no. 3, pp. 341–343, Mar. 1954.
[45] M. C. Teich, T. Tanabe, T. C. Marshall, and J. Galayda, "Statistical properties of wiggler and bending-magnet radiation from the Brookhaven vacuum-ultraviolet electron storage ring," *Phys. Rev. Lett.*, vol. 65, p. 3393, Dec. 1990.
[46] I. Lobach, S. Nagaitsev, V. Lebedev, A. Romanov, G. Stancari, A. Valishev, A. Halavanau, Z. Huang, and K.-J. Kim, "Transverse beam emittance measurement by undulator radiation power noise," *Phys. Rev. Lett.*, vol. 126, no. 13, Apr. 2021, Art. no. 134802.
[47] A. Andreychenko, A. J. E. Raaijmakers, A. Sbrizzi, S. P. M. Crijns, J. J. W. Lagendijk, P. R. Luijten, and C. A. T. Van Den Berg, "Thermal noise variance of a receive radiofrequency coil as a respiratory motion sensor," *Magn. Reson. Med.*, vol. 77, no. 1, pp. 221–228, Jan. 2017.
[48] N. Wiener, "Generalized harmonic analysis," *Acta Math.*, vol. 55, no. 1, pp. 117–258, Dec. 1930.
[49] A. Khintchine, "Korrelationstheorie der stationären stochastischen Prozesse," *Mathematische Annalen*, vol. 109, pp. 604–615, May 1934.
[50] K. S. Roy, J. Sharma, S. Kumar, and M. R. Kumar, "Effect of coronavirus lockdowns on the ambient seismic noise levels in Gujarat, Northwest India," *Sci. Rep.*, vol. 11, p. 7148, Mar. 2021.
[51] A. Secco, A. Tonin, A. Rana, A. Jaramillo-Gonzalez, M. Khalili-Ardali, N. Birbaumer, and U. Chaudhary, "EEG power spectral density in locked-in and completely locked-in state patients: A longitudinal study," *Cogn. Neurodyn.*, vol. 15, pp. 473–480, Oct. 2021.
[52] R. Ackermann, F. Wiekhorst, A. Beck, D. Gutkelch, F. Ruede, A. Schnabel, U. Steinhoff, D. Drung, J. Beyer, C. Abmann, L. Trahms, H. Koch, T. Schurig, R. Fischer, M. Bader, H. Ogata, and H. Kado, "Multichannel SQUID system with integrated magnetic shielding for magnetocardiography of mice," *IEEE Trans. Appl. Supercond.*, vol. 17, no. 2, pp. 827–830, Jun. 2007.
[53] M. Cerna and A. F. Harvey, "The fundamentals of FFT-based signal analysis and measurement," Nat. Instrum., Austin, TX, USA, Appl. Note 041, 2000.
[54] G. Heinzel, A. Rüdiger, and R. Schilling, "Spectrum and spectral density estimation by the discrete Fourier transform (DFT), including a comprehensive list of window functions and some new flat-top windows," *Max-Planck-Inst*, vol. 12, 2002.
[55] E. R. Wooliams, "Determining the uncertainty associated with integrals of spectral quantities," Metrol. Solid State Lighting, Teddington, U.K., Tech. Rep. EMRP-ENG05-1.3.1, Version 1.0, 2013.
[56] J. Leliaert, A. Vansteenkiste, A. Coene, L. Dupré, and B. Van Waeyenberge, "Vinamax: A macrospin simulation tool for magnetic nanoparticles," *Med. Biol. Eng. Comput.*, vol. 53, no. 4, pp. 309–317, Apr. 2015.
[57] K. Lasocha and D. Alves, "Estimation of longitudinal bunch characteristics in the LHC using Schottky-based diagnostics," *Phys. Rev. A, Gen. Phys.*, vol. 23, no. 6, Jun. 2020, Art. no. 062803.
[58] A. Coene and J. Leliaert, "Simultaneous coercivity and size determination of magnetic nanoparticles," *Sensors*, vol. 20, no. 14, p. 3882, 2020.
[59] E. L. L. Landau, "Theory of the dispersion of magnetic permeability in ferromagnetic bodies," *Phys. Z. Sowietunion*, vol. 8, p. 153, May 1935.
[60] T. L. Gilbert, "A phenomenological theory of damping in ferromagnetic materials," *IEEE Trans. Magn.*, vol. 40, no. 6, pp. 3443–3449, Nov. 2004.
[61] S. Chandrasekhar, "Stochastic problems in physics and astronomy," *Rev. Mod. Phys.*, vol. 15, no. 1, pp. 1–89, Jan. 1943.
[62] L. B. Kiss, J. Söderlund, G. A. Niklasson, and C. G. Granqvist, "New approach to the origin of lognormal size distributions of nanoparticles," *Nanotechnology*, vol. 10, no. 1, p. 25, 1999.
[63] S. K. Piotrowski, M. F. Matty, and S. A. Majetich, "Magnetic fluctuations in individual superparamagnetic particles," *IEEE Trans. Magn.*, vol. 50, no. 11, pp. 1–4, Nov. 2014.
[64] M. El-Hilo and R. W. Chantrell, "Rationalisation of distribution functions for models of nanoparticle magnetism," *J. Magn. Magn. Mater.*, vol. 324, no. 16, pp. 2593–2595, Aug. 2012.

KATRIJN EVERAERT received the B.S. and M.S. degrees in physics from KU Leuven University, Belgium, in 2017 and 2019, respectively. During her master's degree, she was an Exchange Student with the Physics Department, FU Berlin, Germany. She is currently pursuing the Ph.D. degree with Ghent University in a collaboration with the Physikalish-Technische Bundesanstalt, Berlin. Her research interest includes magnetic nanoparticle characterization.

MAIK LIEBL received the B.Sc. and M.Sc. degrees in biomedical engineering and the Ph.D. degree from the Technical University of Ilmenau, in 2009, 2011, and 2016, respectively. Since 2011, he has been as a Researcher with the Physikalisch-Technische Bundesanstalt, Berlin. He is currently a Postdoctoral Researcher with the Physikalisch-Technische Bundesanstalt. His research interests include software and hardware development of imaging modalities for magnetic micro- and nanoparticles to support their biomedical application.

DIRK GUTKELCH received the master's degree in mechanical engineering from the Physikalisch-Technische Bundesanstalt, The National Metrology Institute, Germany, in 1997. He has long-standing experience in the construction and development of scientific equipment and apparatus for biomedical measurements. His research interest includes technical improvements of subtractive and additive manufacturing methods for plastics in medical imaging.

JAMES WELLS received the M.Phys. degree (Hons.) in physics from the University of Reading, Reading, U.K., in 2009, and the Ph.D. degree in physics from the Royal Holloway College, University of London, London, U.K., in 2014. From 2013 to 2016, he was a Higher Research Scientist with the National Physical Laboratory, London. Since 2016, he has been a Researcher with the Physikalisch-Technische Bundesanstalt, Berlin, Germany. He has authored more than 25 peer-reviewed research articles and one book chapter. His research interests include quantum technologies, nanotechnology and novel medical devices. He is a member of the Institute of Physics.

BARTEL VAN WAEYENBERGE received the master's and Ph.D. degrees in physics from Ghent University, Belgium, in 1995 and 2002, respectively. He joined the Max-Planck-Institute for Metals Research, Stuttgart, Germany, in 2002, working on time-resolved magnetic imaging using X-rays. In 2009, he returned to Ghent University as a Professor in physics and started the research group Dynamat with the Department of Solid State Sciences. He has published more than 80 articles and has supervised six Ph.D. students. He has supervised the development of the widely used micromagnetic code Mumax. His research interests include numerical and experimental study of magnetization dynamics in nanoscale magnetic material and devices.

FRANK WIEKHORST received the Ph.D. degree (Dr.Rer.Nat.) in physics from the University of Hamburg, Germany. He is currently a Leader of the working group Metrology for Magnetic Nanoparticles with the Physikalisch-Technische Bundesanstalt, the National Metrology Institute, Germany. His research interests include development of measurement techniques for characterization, quantification, and imaging of magnetic nanoparticle systems for biomedical applications.

JONATHAN LELIAERT (Member, IEEE) received the M.Sc. and Ph.D. degrees in physics from Ghent University, Belgium, in 2012 and 2016, respectively. He was a Guest Scientist with the Physikalisch-Technische Bundesanstalt, Berlin, Germany, and was selected as an Emerging Leader of *Journal of Physics D: Applied Physics*. He received Postdoctoral Research Fellowships from the Research Foundation Flanders to continue his work at Ghent University, where he co-developed the micromagnetic software package MuMax3. His research interests include nanoscale magnetization dynamics in thin films and nanoparticles.